EEET ECOLOGICAL ENGINEERING & ENVIRONMENTAL TECHNOLOGY

Ecological Engineering & Environmental Technology 2023, 24(1), 125–135
https://doi.org/10.12912/27197050/155058
ISSN 2719-7050, License CC-BY 4.0

Received: 2022.08.25
Accepted: 2022.10.10
Published: 2022.11.01

Landslide Monitoring in the Jebha Region by Radar Permanent Scattered Remote Sensing Technique

Bouchra Azizi[1*], Mustapha Hakdaoui[1], Mohammed Raji[1], Mariam Taazzouzte[1]

[1] Laboratory of Applied Geology, Geomatics and Environment, Hassan II University of Casablanca, Ben M'sik Faculty of Sciences, Casablanca, Morocco

* Corresponding author's e-mail: azizibouchra13@gmail.com

ABSTRACT

The city of Eljebha, Morocco, and its surroundings have always been affected by instability and slope failure, both natural and man-made. The Neogene conglomeratic clay formations, which form most of the city of Constantine, are extremely sensitive to the presence of water, which makes them susceptible to landslides. Therefore, to preserve the environment and endangered species, remote sensing has been designed to facilitate the monitoring and supervision of natural hazards and threats. The present paper deals with the detection of stable points by the new technique of permanent dispersers PSInSAR, as well as the subsidence rate with an accuracy in mm/year in the area of El Jebha in Morocco from 2016 to 2018 using Sentinel 1 complex SLC data in IW mode.

Keywords: remote sensing, PSInSAR, subsidence rate, Sentinel 1, SLC, IW mode.

INTRODUCTION

Landslides are natural hazards that have a significant impact worldwide (IGOS, 2004), they are defined as the displacement of a mass of rock, debris or soil along a slope under the influence of gravity (Cruden, 1996) and are triggered by natural phenomena such as earthquakes, heavy rainfall, volcanic eruptions, or by human activities such as logging or road construction, or both (Dai and Lee, 2002).

These landslides have a significant impact on the entire road network, which is subject to frequent degradation. This requires regular identification and monitoring of landslides to maintain the network in good condition, which is often costly (About 50% of the total budget allocated to the DPET in the Rif is spent on road reinforcement and rehabilitation works following landslides (Rmili and Janati, 1995).

The province of El Jebha is located in the North of Morocco on the Rif Mountain range, on its Mediterranean coast. In terms of severity and frequency of ground movements, it ranks first among the other provinces. The intensity of this In parallel, several studies have focused on mapping landslide vulnerable areas using GIS methods (Mastere et al., 2015; El Fahchouch et al., 2015). The creation of a regional landslide inventory map is therefore at the core of landslide investigation and research (Harpe et al., 2011; Du et al., 2020).

The first landslide inventory maps were mainly based on traditional geological field studies (Galli et al., 2008; Pellicani, 2015). Nowadays, remote sensing by optical satellite images (Nichol et al., 2005, Fiorucciet al., 2011), aerial images by drone (Jaboyedoff et al., 2012), airborne LiDAR remote sensing (Görüm et al., 2019; Xu et al., 2021; Wasowski et al., 2014), InSAR monitoring, persistent scatterer interferometry (PSI) (Ferretti et al., 2000; Berardino et al., 2002; Scaioni et al., 2014; Zhang et al. 2021), and other advanced technical methods are used to create Landslide Inventory Maps. As a cost-effective and efficient monitoring method, InSAR technology has been widely used in landslide identification and deformation monitoring (Yao et al., 2019; Yao et al., 2020). It is also of great importance for landslide induction factors, rupture time prediction and risk assessment.

This paper focuses on the detection of subsidence and landslide measurements on the one hand, and on the other hand on the subsidence velocity with an accuracy of cm/year by means of stable point detection. This new persistent scatterer technique "PSInSAR" in the El Jebha region of Morocco, uses complex SLC data from Sentinel 1 in IW mode in a time interval from 2016 to 2018, with the aim of preserving the environment and species threatened by the unpredictable turns of nature in the region.

STUDY AREA

El Jebha is a small Moroccan port town, located on the border of the Eastern and Western Rif of Morocco. It is the urban centre of the rural commune of M'Tioua, in the province of Chefchaouen (Tangier-Tetouan-Al Hoceima region) (Figure 1). However, we took the entire national road RN16 that leads to Amtar and Masstasa, known for its long movements of the terrain.

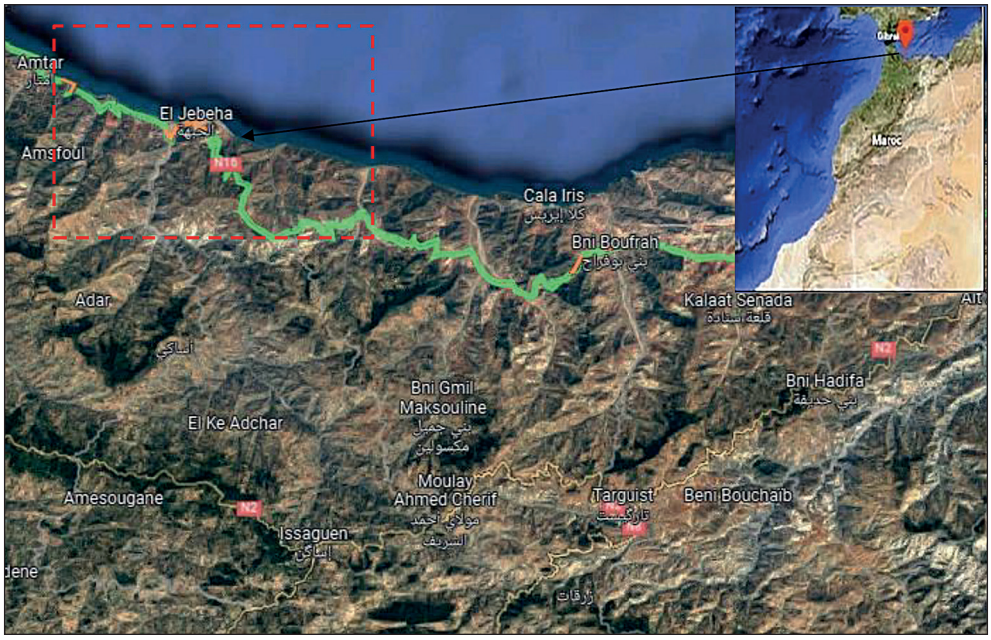

Figure 1. Geographical location of the study area

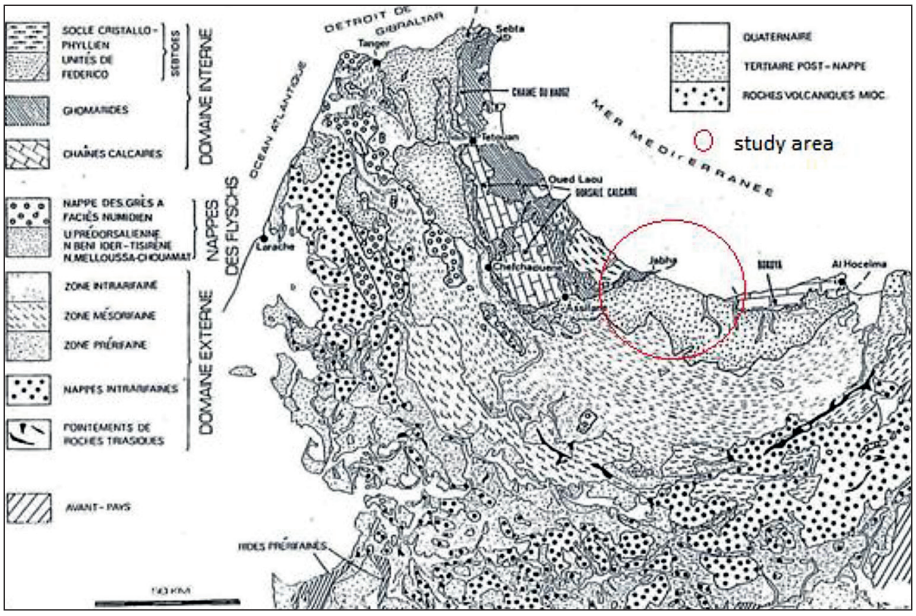

Figure 2. Structural map of the study area (Suter, 1980)

Geological, structural and hydrogeological setting of the area

The Rif, a mountainous edifice in the northern part of Morocco, is one of the alpine chains around the western Mediterranean, in terms of its age and style (Lespinasse, 1975). It comprises, above the elements of the ancient basement, a secondary and tertiary sedimentary series. Its structure, as shown in (Figure 2), includes multiple and intense folding, accompanied by metamorphism, as well as significant over thrusting and thrusting towards the west and south-west (Michard, 1976). Indeed, in the western part of the RIF, the Cretaceous presents marly-limestone formations, which rest on the Beni Ider marls of Oligocene age, Eocene marls and then on the Paleozoic formations rich in garnet and mica schists especially at the level of Jbel Moussa, and the Sebta promontory linked to the important metamorphism that the region has experienced (Limam al., 2012)

The Eljebha area belongs to the eastern Mediterranean where we find rather the sandstone-molassic of the Miocene and the schist and sandstone nappes and conglomerate of the Paleozoic with the dominance of cliffs Plioquaternary (Limam et al., 2012). The center of the study area is occupied by the limestone ridge, which constitutes the most important karstic aquifer in the whole Rifa domain (Amraou et al., 1988). In addition to this aquifer, there are several thrust sheets that testify to the important tectonisation that the study area has undergone (Amraou et al., 1988).

MATERIALS AND METHODS

SAR radar interferometry

Radar interferometry consists of exploiting the phase information contained in complex SAR images recorded by one or more sensors, by varying an acquisition parameter (date, position and orientation of the radar, frequency, polarity of the transmitted/received wave) according to the desired application (Bamler and Hartl, 1998). This broad definition allows for the inclusion of all methods and applications of interferometry.

Landslides can be detected and even monitored in the case of slow, regular and large area movements (Fruneau et al., 1995; Manunta et al., 2006). This technique can also be used to detect subsidence related to human activities, such as mining subsidence (Sandwell et al., 2000), settlement of porous formations by the exploitation of fluids, such as water, gas and oil (Fielding et al., 1998; Rabus et al., 2004).

Stable point interferometry

The persistent scatterers interferometry (PS) technique, hereafter referred to as the PSI method, was scientifically developed at the Politecnico di Milano (POLIMI) in 1999 (Ferretti, 2001). Numerous approaches started to be developed from the end of the 1990s to try to solve the problems of the differential method and to make the best use of the databases provided by SAR satellites (Usai et al. 1999, Ferretti et al. 2000, 2001, Berardino et al. 2002, Schmidt and Bürgmann, 2003). These approaches, using several acquisitions on the same scene, allow to improve the accuracy of the measurements and to follow in time the evolution of the backscattering wedge displacements.

Over the past decades, persistent scattering interferometry (PSI) has proven to be a powerful tool for measuring and monitoring deformation. This technique uses large stacks of interferometric SAR images to derive deformation maps and deformation time series. In this paper, Sentinel-1 images are used to derive deformation monitoring.

Other calculation methods using the principle of persistent reflectors now exist. This is the case of the approaches developed by (Hooper et al. 2004) at Stanford University STAMPS, which we use in our work (Kampes, 2006) at DLR in collaboration with the University of Delft (STUN), Werner et al. (2003) and his Gamma team in Switzerland (IPTA), and by (Arnaud, 2003) in his company Altamira Information, with the InSAR Stable Points Network (InSAR SPN). The PSI technique is also being exploited industrially and commercially by TRE Tele Rilevemento Europa (a POLIMI start-up) with the PSInSAR™ patent (POLIMI patent 1999).

PSI analysis is generally based on linear displacement models, i.e. displacements with relatively constant deformation rates over the observation period. While it is possible to a certain extent to describe non-linear displacements with these methods, profiles will be rejected or judged to be of poor quality because the linear model is not sufficient to allow the tracking of a non-linear phenomenon over time. The challenge is now to design a specific treatment based on a non-linear model, adapted to non-continuous displacements in time.

The original version of Stamps, which is an algorithm with a non-linear displacement model and which we use in this work, was developed at Stanford University, but was subsequently developed at the University of Iceland, Delft University of Technology and the University of Leeds.

These reflectors are said to be «stable» not in the sense that they are immobile over time, but stable in the sense that they are sufficiently backscattering so that the phase of the dominant signal can be studied: thanks to the redundancy of information, brought about by the use of several interferograms, it is possible to reduce the noise on the measurements and to separate the phase term linked to the deformation from the rest of the interferometric signal. In the scientific literature, the term permanent points is also used, which is considered less ambiguous.

Principle

The accuracy of measurements obtained by differential interferometry is limited when studying small displacements: on the one hand because of the loss of coherence, and on the other hand because of atmospheric contributions which mask the phase signal linked to the displacement, thus limiting its application to the study of deformations with a sufficiently large magnitude. Furthermore, the monitoring of the temporal evolution of a deformation that is not regular in time remains problematic: using differential interferometry, a phase difference diagram is calculated between two radar images, which, once unrolled, gives information on the cumulative displacements between the two acquisition dates. However, the intermediate acquisitions available are not necessarily usable, because of the perpendicular and/or temporal baselines being too large.

The aim of PSI is therefore to exploit a series of SAR radar data while avoiding the limitations of differential interferometry such as temporal and geometric decorrelations and phase shifts due to atmospheric effects.

The principle of the method is to select particular points, the PS, whose radar response is sufficiently strong and continuous in time. These reflecting radar points are called "stable" not because their behaviour of the ground surface they represent is immobile or monotonous in time, but stable in the sense that they are sufficiently reflective points to allow the calculation of the phase shift related to the movements of the reflectors over time.

From a series of N+1 SAR images available on the scene of interest (usually more than 20), the amplitude dispersion index is calculated on each pixel (Ferretti et al., 2001):

$$D_A = \frac{\sigma_A}{m_A} \tag{1}$$

where: σ_A and m_A – correspond respectively to the standard deviation and the average of the amplitude of a pixel in time. The selection of the pixels that will be used subsequently is carried out by thresholding on this index (generally taken to be less than 0.25).

The next step is the formation of differential interferograms: from the N+1 SAR images, N interferograms are constructed, by interfering each of the images with a single master image. The choice of the master image is made in such a way as to limit the dispersion of the perpendicular baselines (Colesanti et al., 2003). At each pixel of a given interferogram, the interferometric phase is written as:

$$\emptyset = \emptyset_{\text{topo}} + \emptyset_{\text{dep}} + \emptyset_{\text{atm}} + \emptyset_{\text{bruit}} \tag{2}$$

where: $\emptyset_{\text{topo}}$ – the topography phase;
$\emptyset_{\text{dep}}$ is the point displacement phase;
$\emptyset_{\text{atm}}$ is the atmospheric phase delay;
$\emptyset_{\text{bruit}}$ – decorrelation noise.

The differential interferometric phase, obtained after removing the topographic phase component (simulated from the DTM) is written as:

$$\emptyset = \emptyset_{\text{erreur}} + \emptyset_{\text{topo}} + \emptyset_{\text{dep}} + \emptyset_{\text{atm}} + \emptyset_{\text{bruit}} \tag{3}$$

where: $\emptyset_{\text{erreur\_topo}}$ – the phase delay due to errors in the DTM (the DTM not being perfect). The residual topography phase is proportional to the baseline B_{perp} and the topography error:

$$\emptyset_{\text{erreur\_topo}} = K_1 B_{\text{perp}} \varepsilon_{MNT} \tag{4}$$

where: K_1 a constant, and ε_{MNT} the elevation of the point relative to the reference topographic surface, called the DTM error. A linear model is used to model the displacement:

$$\emptyset_{dép} = K_2 T_k v \tag{5}$$

where: K_2 – a constant;
T_k – the time interval of the pair (or time baseline relative to the master image),
v – the average displacement rate of the point (subsidence rate).

The interferometric phase can therefore finally be expressed as follows:

$$\emptyset = K_1 B_{\text{perp}} \varepsilon_{MNT} + K_2 T_k v + \emptyset_{\text{residu}} \quad (6)$$

where: $\emptyset_{\text{residu}}$ – the phase residual, including noise, atmospheric effects and non-linear displacement of the point, i.e. not taken into account by the term $T_k v$.

The problem remains the phase unwinding. To unwind the phase, we have to estimate the phase difference between neighbouring pixels:

$$\Delta\emptyset = K_1 B_{\text{perp}} \Delta\varepsilon_{MNT} + K_2 T_k \Delta v + \Delta\emptyset_{\text{residu}} \quad (7)$$

By considering pixels that are close to each other, i.e. whose distance is less than the correlation distance of the atmosphere (about 1000 m), it can be assumed that their atmospheric phase is identical. If the residual displacements are similar between neighbouring pixels, then $\Delta\emptyset_{\text{residu}}$ will a priori be less than If these conditions are met, then it is possible to determine DTM $\Delta\varepsilon$ and Δv directly from the set of unrolled interferograms (DTM $\Delta\varepsilon$ and Δv are identical over the whole set of interferograms).

Once this estimate is made, an integration process is used to determine the velocity v and the DTM error for each SP. The residual phase, after elimination of the previous linear deformation terms and DTM error, is calculated for each PS:

$$\emptyset_{\text{residu}} = \emptyset_{\text{dep\_non\_linèaire}} + \emptyset_{\text{atm}} + \emptyset_{\text{bruit}} \quad (8)$$

Finally, this unwound phase residual is filtered to isolate the atmospheric component and the non-linear displacements. The atmospheric phase residuals are assumed to be decorrelated in time, and to have smooth spatial variations. The residual (non-linear) displacements are assumed to be correlated in time and space. High-pass temporal filtering (to remove time-correlated displacement terms), followed by low-pass spatial filtering gives an estimate of the long-wave atmospheric effects. Low temporal frequencies provide an estimate of non-linear displacements. In the end, an estimate of the linear deformation, the DTM errors and the non-linear deformation is obtained for each SP. The PSI method thus provides a network of points on which the evolution of the relative altitude of the reflector displacements along the satellite line of sight can be followed, with the temporal sampling of these measurements corresponding to the dates of the image acquisitions.

Compared to the classical DinSAR method, which uses radar image pairs to estimate ground surface displacements in a stepwise fashion, the PSI method provides displacement information for each target continuously over time, which is more useful for tracking and thus understanding discrete reflector movements.

One of the major advantages of the method is the elimination of the atmospheric component (Duro, 2009). It also eliminates temporal and geometric decorrelation, as only the most coherent and suitable portions of the SAR image for the interferometric application are computed.

In addition, the post-processing of PSI data is less important than in the case of the DinSAR method, which loses part of its information during filtering or ortho-rectification, which is necessary for its interpretation. The accuracy of the measurement is thus significantly improved compared to DinSAR.

Download Sentinel 1A and 1B images

To do interferometry and have good interferograms it is necessary to work with images having a parallel polarisation, however, for our area we have an availability of IW data having a double polarisation VV VH, indeed, the VV polarisation responds more to the vertically oriented structures than HH notably the vegetation and the urban areas what can lead us not to have a lack or loss of PS for our final result. The optimal use of single and dual polarisation acquisitions is dependent on the available downlink capacity and for broadband interferometric (IW) modes, they operate in pre-defined geographical areas:

- On land and coastal areas: the predefined mode is IW.
- On seas and polar areas and areas affected by the ocean, the preset mode is IW or EW.

The optimal use of single and dual polarisation acquisitions is dependent on the available downlink capacity and for broadband interferometric modes. The table below (Table 1) provides a summary of the years of acquisition, satellite, sensor, product type, polarisation and the mode of acquisition of our data.

We used 8 images in 2017 to measure the ground subsidence velocity in the area and detect SP and 12 images in each year (2016, 2017, 2018) shared over the 12 months of the year from January to December. Sentinel images are made available free of charge by ESA via the websites.

Table 1. Description of images used for the PSI method of the study area

Satellite	Years of acquisition	Sensor	Type of product	Polarisation	Mode of acquisition
Sentinel 1-A Sentinel 1-B	2016 2017 2018	SAR-C	SLC	VV and VH	IW

Pre-processing and processing

The preparation of a PS calculation with STAMPs on SNAP is done in different steps illustrated in the following diagram (Figure 3). The steps are described in the section below:

- step 1 – selection of the area of interest bursts from the IW2 subswath;
- step 2 – taking into account the orbit data;
- step 3 – registration of the images to each other. The images must be re-aligned to become superimposable. The first image chosen will be the master image used as a reference for the other images, this one was chosen by the 'INSAR STACK OVERVIEW' tool;
- step 4 – creation of interferograms. This step aims to create a stack of interferograms from the stack of images recalculated in the previous step;
- step 5 – removal of horizontal black bands – Deburst. This step is used to remove the black bands. It is applied to the stack of interferograms obtained in step 4 and to the stack of images recalculated in step 3;
- step 6 – preparation of the input data for StaMPS.

Next, we will prepare the python script: We were able to develop the coregistration and interferogram creation step using the gpt (graph processing tool) library and based on the Snap-2Stamps module. The coregistration and interferograms were developed in a single python code.

Processing with STAMPS

StaMPS (Standford Method for Permanent Scatterer) is a software package that uses spatial phase correlation in interferograms to find PSs, i.e., phase-stable pixels. These PS allow the study of the deformations of an area. To do this, StaMPS needs to be provided with the initial data, i.e., the interferograms.

The first step is to prepare MATLAB by calling the script mt_prep_snap.py in the results folder obtained during the stamps export while entering the parameters corresponding to the following calculation elements:

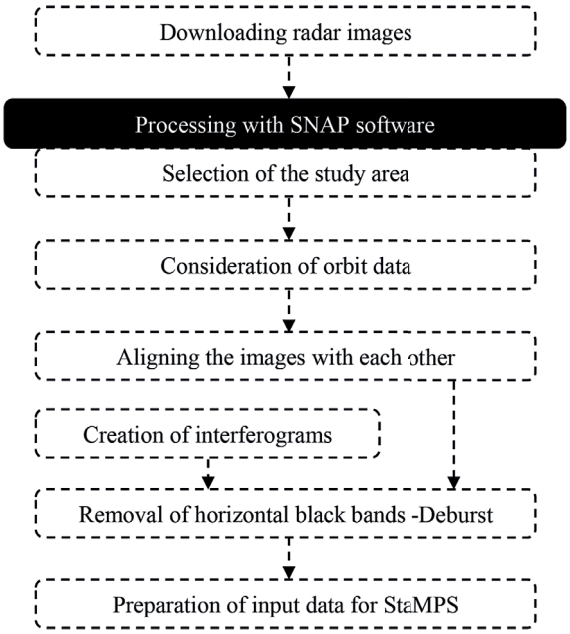

Figure 3. Diagram showing the different PS calculation step

- threshold on the average amplitude of a pixel divided by the standard deviation (0.4 is the default value). For a first PS detection;
- number of patches in range;
- number of patches in azimuth;
- number of common pixels between patches in range;
- number of common pixels between patches in azimuth.

Processing with Matlab

The first step is to prepare matlab by calling the scipt mt_prep_snap.py in the results folder obtained during the stamps export while entering the parameters corresponding to the following calculation elements: The number of PATCHs chosen depends on both the size of the area under study and the computer's memory. It is assumed that a patch should contain less than 5 million pixels.

- step 1 – select data in the required formats for SP processing;
- step 2 – estimation of the phase noise for each pixel that can be a PS;

- step 3 – selection of SPs;
- step 4 – weeding of the PS;
- step 5 – phase correction;
- step 6 – unwrapping the phase;
- step 7 – estimation of the spatially correlated view angle error;
- step 8 – spatially correlated noise filtering.

Processing with Snaphu

After phase filtering and using the accurate background information, the unwrapped interferograms generated a height map by calculating the vertical displacement from equation (9):

$$d_{\text{vertical}} = -\frac{\lambda}{4\pi\, cos(\text{incident angle})}\Delta\emptyset \quad (9)$$

RESULTS

The ground subsidence rate over the selected area varies between -51.6 mm to 162 mm for a duration between 12 January 2017 and 22 December 2017. More specifically in El Jebha the velocity is approximately between 42.3 mm and 149.1 mm. In general, there is an increasing subsidence rate east of Jebha (reaching -51.6 mm) and west of Jebha reaching 162 mm (Figure 4).

A comparative analysis of the velocity according to the dates of the input data can be made from the stamps visualizer in the form of a diagram. As can be seen from the diagram (Figure 5) the velocity reached its maximum for the year 2017 in April and its minimum between April and June (Figure 6).

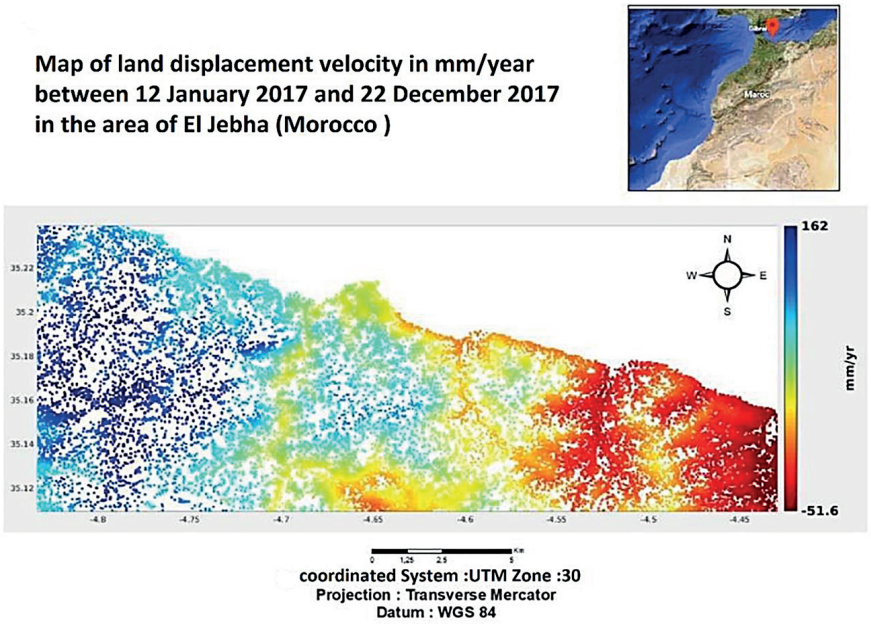

Figure 4. Map of 2017 ground subsidence rate in El Jebha Morocco area in mm/year

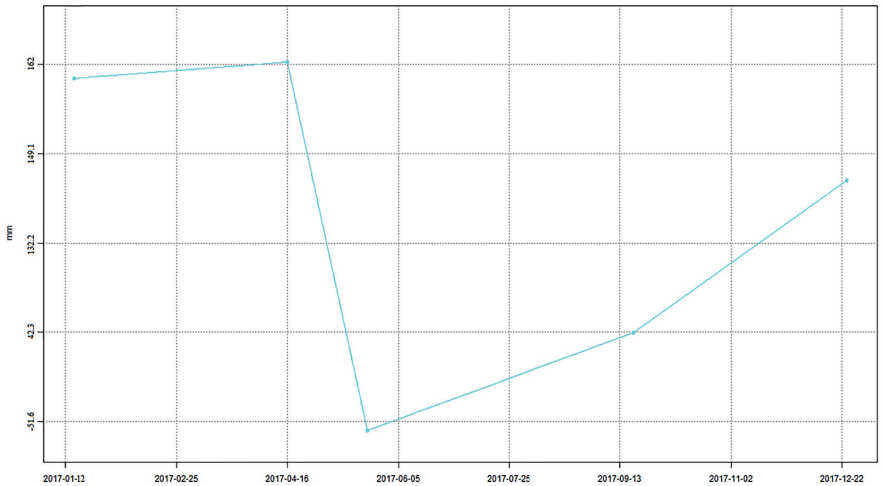

Figure 5. Comparison chart of subsidence velocities from the 2017 data acquisitions

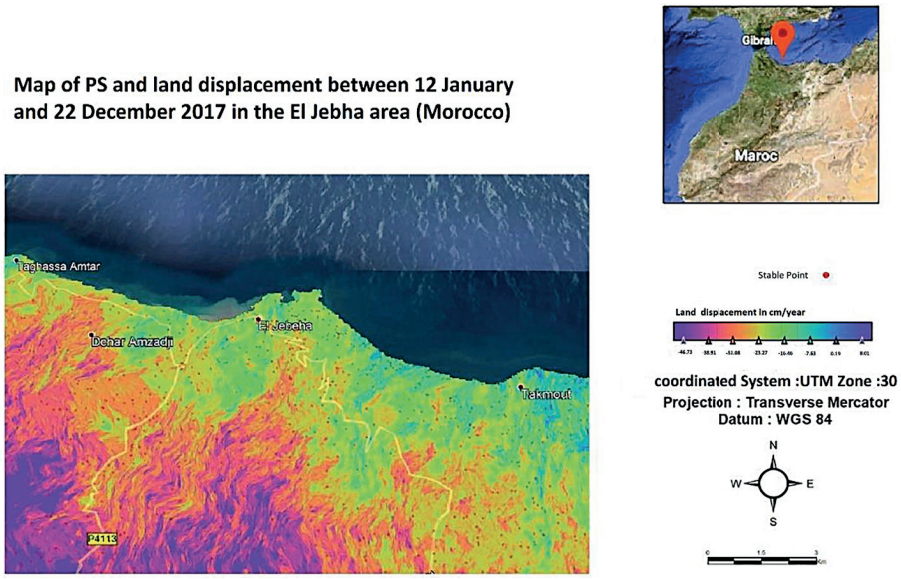

Figure 6. Map of PS and field displacement of the year 2017 in the El Jebha area

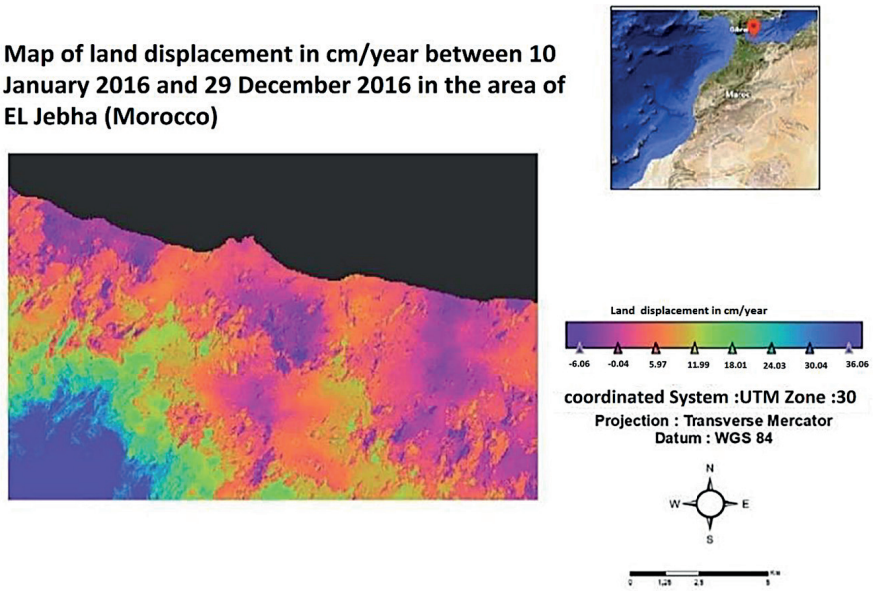

Figure 7. Land displacement map of the year 2016 in the El Jebha area in cm

The stable points

The PS obtained are the points that are sufficiently backscattering to study the phase of the dominant signal: thanks to the redundancy of the information, brought by the fact of using several interferograms. This gives the points where the displacement result is most reliable and least ambiguous. In 2017, the displacement is between -14.92 cm and 1.06 cm. The displacement is greatest in the area of RN16 towards Amtar where a slope failure occurred in late May 2017.

For the year 2016 the results of the land displacement in El Jebha vary between -6.06 and 5.97 cm. The subsidence is increasingly strong in the south of Jebha. It can be seen that there are three large areas where the landslide reaches -6.06 cm which we have represented below (Figure 8). For the year 2018, the displacement is between -14.28 cm and 2.21 cm. In Figure 10 we present the large areas where there was a landslide reaching -14.28, which is located east and west of El Jebha.

Through this work, we were able to overcome the limitations of the differential interferometry technique and produce a tool that optimises the entire data preparation phase for processing that can be used for years to come.

The PSInSAR technique makes it possible to exploit a series of SAR radar data while overcoming the limitations of differential interferometry

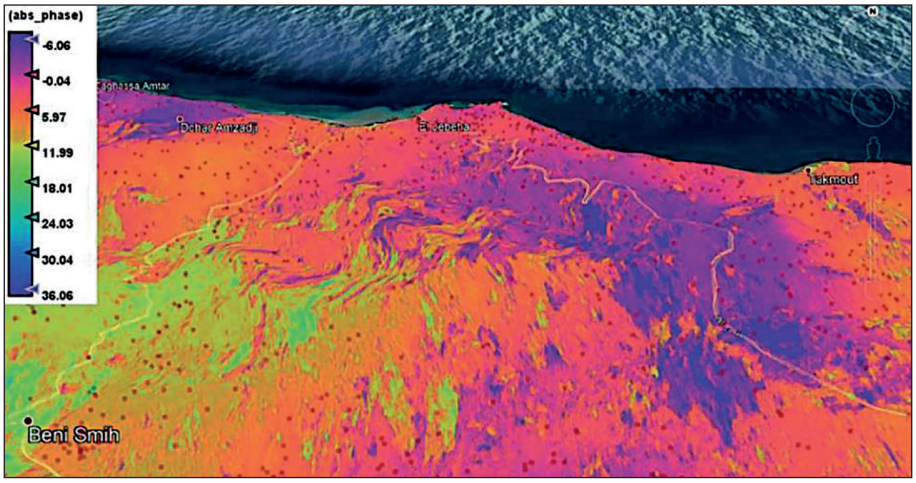

Figure 8. Visualisation with Google Earth Pro

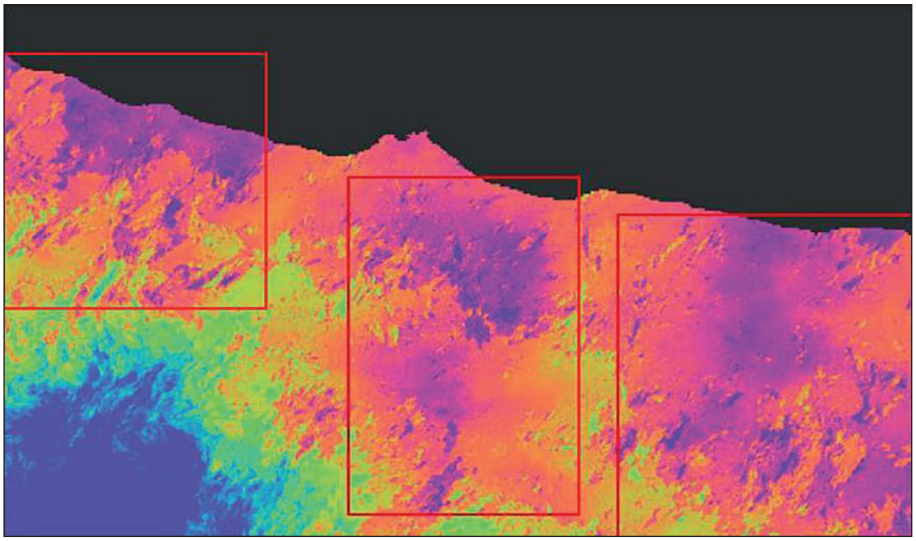

Figure 9. Strong landslide 2016

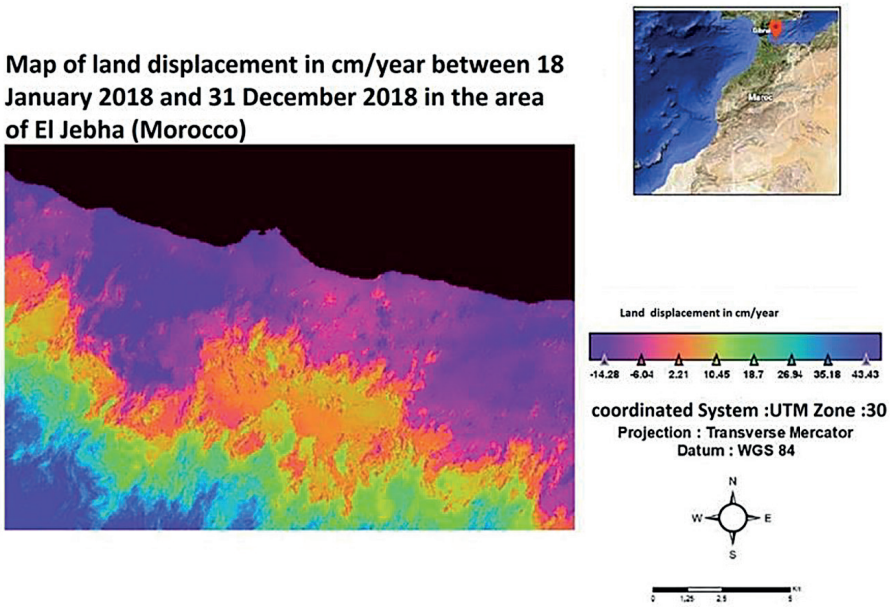

Figure 10. Land displacement map of the year 2018 in the El Jebha area in cm

such as temporal and geometric decorrelations and phase shifts due to atmospheric effects. By selecting particular points, SPs with a sufficiently strong and continuous radar response over time. These reflecting radar points are called "stable" not because their behavior of the ground surface they represent is immobile or monotonous in time, but stable in the sense that they are sufficiently reflective points allowing the calculation of the phase shift related to the movements of the reflectors over time.

This difference between the years can be explained in addition to the nature of the rock by the non-constant characteristics favoring the sliding such as the climate (rainfall, temperature), seismic activities, land use (as the area is under construction). In fact, a diagnostic study on its effects must be carried out, which opens doors for new projects. On the other hand, it is necessary to know that in order to carry out an analysis of the permanent dispersers more images must be available (usually at least 25–30), in order to correctly identify the SPs with statistical indices and to correctly estimate the values of Δv and $\Delta \varepsilon$.

CONCLUSIONS

The study area in this paper has a high frequency of landslides, the displacement is greater in the area of RN16 going to Amtar, so the subsidence is increasingly strong south of El Jebha, due to Due to the rugged topography the vulnerable geo- technical nature of the soil, and the activity of its saturated and watered soil (heavy rainfall and important presence of springs), Therefore, the maintenance of retaining walls and the evacuation of rainwater are important remains a reliable solution to ensure the safety of the traffic comfortably.

REFERENCES

1. Amelung F., Galloway D.L., Bell J.W., Zebke H.A. 1999. Sensing the ups and downs of Las Vegas: InSAR reveals structural control of land subsidence and aquifer-system deformation, pubs.geoscienceworld.org
2. Amraoui A. 1988. Geology of the Rif limestone ridge (Northern Morocco), PhD thesis.
3. Bamler R., Hartl P. 1998. Synthetic aperture radar interferometry. Inverse problems. iopscience.iop.org
4. Berardino P., Fornaro G., Lanari R. 2002. A new algorithm for surface deformation monitoring based on small baseline differential SAR interferograms, IEEE Transactions. ieeexplore.ieee.org
5. Berardino P., Fornaro G., Lanari R., Sansosti E. 2002. A new algorithm for surface deformation monitoring based on small baselin.
6. Chalouan A. 1986. Les nappes ghomarides (Rif septentrional Maroc). Un terrain varisque dans la chaîne alpine. PhD thesis, Univ. Louis Pasteur, Strasbourg.
7. Colesanti C., Ferretti A., Prati C., Rocca F. 2003. Monitoring landslides and tectonic motions with the Permanent Scatterers Technique, Engineering geology, Elsevier.
8. Cruden D.M., Varnes D.J., 1996. Landslide types and processes. In: Turner A.K., Schuster R.L.(Eds.), Landslides: Investigation and Mitigation, Sp.Rep.247, Transportation Research Board, National Research Council, National Academy Press, Washington DC, pp. 36–75.
9. Dai F.C., Lee C.F. 2002. Lands lide characteristics and slope in stability modeling using GIS, Lantau Island, Hong Kong. Geomorphology 42, 213–228.
10. Du J., Glade T., Woldai T., Chai B., Zeng B. 2020. Évaluation de la sensibilité aux glissements de terrain basée sur un inventaire incomplet des glissements de terrain dans la vallée de Jilong, au Tibet, dans l'Himalaya chinois. Ing. Géol., 270, 105572.
11. El Fahchouch A.N., Brahim L.A., Raji O., Khouakhi A. 2015. Apport du SIG et de la télédétection dans la modélisation spatiale de la susceptibilité aux mouvements de terrain dans la région d'Al Hoceima, Rif Oriental, Maroc. Afrique Science, 11(2), 44–57.
12. El Fellah B. 1994. Eboulement rocheux dans le Paléozoïque du Rif : Présentation d'un cas sur la route Oued Lao-Jebha. 7Eme Congrès International de l'AIGI, Lisbon, Portugal, 3927–3931.
13. Ferretti A., Prati C., Rocca F. 2000. Nonlinear subsidence rate estimation using permanent scatterers in differential SAR interferometry. IEEE Trans. Geosci. Remote Sens., 38(5), 2202–2212.
14. Ferretti A., Prati C., Rocca F. 2001. Permanent scatterers in SAR interferometry. IEEE Transactions on geoscience, ieeexplore.ieee.org
15. Fielding E.J., Blom R.G. 1998. Rapid subsidence over oil fields measured by SAR interferometry, Geophysical research, Wiley Online Library.
16. Fiorucci F, Cardinali M., Carla R., Rossi M., Mondini A.C., Santurri L., Ardizzone F., Guzzetti F. 2011. Cartographie des glissements de terrain saisonniers et estimation des taux de mobilisation des glissements de terrain à l'aide d'images aériennes et satellitaires. Géomorphologie, 129, 59–70.
17. Fruneau B., Achache J. 1995. Détection du glissement de terrain de Saint-Etienne-de-Tinée par interférométrie SAR et modélisation, l'Académie des sciences. Série 2, pascal-francis.inist.fr
18. Galli M., Ardizzone F., Cardinali M., Guzzetti,

F., Reichenbach P. 2008. Comparaison des cartes d'inventaire des glissements de terrain. Géomorphologie, 94, 268–289.

19. Görüm T. 2019. Reconnaissance et cartographie des glissements de terrain dans un environnement forestier mixte à partir de données LiDAR aéroportées. Ing. Géol., 258, 105155.
20. Hanssen R.F., 2001. Radar interferometry: data interpretation and error analysis - books.google.com
21. Harpe E.L., Keefer D.K., Sato H.P., Yagi H. 2011. Inventaires des glissements de terrain: la partie essentielle des analyses des risques de glissement de terrain sismique. Ing. Géol., 122, 9–21.
22. Hooper A., Zebker H., Segall P. 2004. A new method for measuring deformation on volcanoes and other natural terrains using InSAR persistent scatterers, Geophysical research, Wiley Online Library.
23. IGOS, 2004. Geohazards theme report for the monitoring of our environment from Space and from Earth. European Space Agency Publication, Rome (Italy), p.55.
24. Jaboyedoff M., Oppikofer T. ,Abellán A., Derron M.H., Loye A., Metzher R., Pedrazzini 2012. A. Utilisation du LiDAR dans les enquêtes sur les glissements de terrain: un examen. Nat. Dangers, 61, 5–28.
25. Kampes, 2006. Radar Interferometry with Public Domain Tools Bert M.
26. Lespinasse P. 1975. Géologie des zones externes et des flyschs entre Chaouen et Zoumi (Centre de la chaîne rifaine, Maroc). Thèse d'Etat, Sciences Naturelles, Univ. Paris, 231.
27. Limam A. 2012. Summary report of the "priority" list of sites deserving protection on the mediterranean coast in Morocco, Projet MedMPAnet, CAR/ASP.
28. Massonnet D., Feigl K.L. 1995. Discrimination of geophysical phenomena in satellite radar interferograms. Geophysical Research Letters, Wiley Online Library.
29. Massonnet D., Feigl K.L. 1998. Radar interferometry and its application to changes in the Earth's surface. Reviews of geophysics, Wiley Online Library.
30. Massonnet D., Rossi M., Carmona C., Adragna F. 1993. The displacement field of the Landers earthquake mapped by radar interferometry, nature.com
31. Mastere M., Lanoë B., Ait Brahim B., El Moulat M.A. 2015. Linear indexing approach to mass movements susceptibility mapping. Revue Internationale de géomatique, 25(2), 245–265.
32. Meziane S. 2019. Study of landslides in mediterranean bypass road, case of Jebha. ARPN Journal of Engineering and Applied Sciences, 14(21), 3688-93.
33. Michard A. 1976. Elements of Moroccan geology. Notes and Mem. Serv. Carte géol. Morocco, 252, 408 p. In: Sciences Géologiques. Bulletin, volume 29, n°4, 1976. Sedimentology and geochemistry of the surface.
34. Nichol J. ,Wong M.S. 2005. Détection et interprétation des glissements de terrain à l'aide d'images satellitaires. Terrain Degrand, 16, 243–255.
35. Manunta M., Nichols B.J., Tan P.H., Sagoo P. 2006. Gene delivery by dendrimers operates via different pathways in different cells, but is enhanced by the presence of caveolin. Journal of Immunological Methods, 314(1–2), 134-146.
36. Pathier E., Leijen F.V., Hanssen R. 2005. Measuring interseismic deformation across the North Anatolian fault: Comparison of InSAR techniques – AGU Fall Meeting, ui.adsabs.harvard.edu
37. Peltzer G., Rosen P. 1995. Surface displacement of the 17 May 1993 Eureka Valley, California, earthquake observed by SAR interferometry, science.org
38. Rmili A. 1995. La démarche qualité au sein de la direction des routes et de la circulation routière. Civil engineering; Transportation, 8, 81(2), 48–51.
39. Sandwell D.T., Sichoix L., Agnew D. 2000. Near real-time radar interferometry of the Mw 7.1 Hector Mine earthquake, Geophysical, Wiley Online Library.
40. Scaioni M., Longoni,L., Melillo V., Papini M. 2014. Télédétection pour les enquêtes sur les glissements de terrain: Un aperçu des réalisations récentes et des perspectives. Remote Sens., 6, 9600–9652.
41. Schmidt D.A., Bürgmann R. 2003. Time-dependent land uplift and subsidence in the Santa Clara valley, California, from a large interferometric synthetic aperture radar data set. Journal of Geophysical Research, Wiley Online Library.
42. Suter G. 1980. Carte géologique de la chaîne rifiane à 1/500.000. Notes et Mém. Serv. géol. Maroc, 245a.
43. Usai R., Klees. 1999. SAR interferometry on a very long-time scale: A study of the interferometric characteristics of man-made features. IEEE Transactions on Geoscience. ieeexplore.ieee.org
44. Wasowski J., Bovenga F. 2014. Enquête sur les glissements de terrain et les pentes instables avec l'interférométrie multi-temporelle par satellite: Problèmes actuels et perspectives futures. Ing. Géol., 174, 103–138.
45. Xu Q., Guo C., Dong X., Li W., Lu H., Fu H., Liu X. 2021. Cartographie et caractérisation des déplacements de glissements de terrain avec les technologies InSAR et LiDAR aéroporté: Une étude de cas du comté de Danba, dans le sud-ouest de la Chine. Remote Sens., 13, 4234.
46. Zebker H.A., Rosen P.A., Goldstein R.M. 1994. On the derivation of coseismic displacement fields using differential radar interferometry: The Landers earthquake, Wiley Online Library.
47. Zhang L., Dai K., Deng J., Ge D., Liang R., Li, W., Xu Q. 2021. Identification des glissements de terrain potentiels par empilement-InSAR dans le sud-ouest de la Chine et comparaison de ses performances avec SBAS-InSAR. Remote Sens., 13, 3662.